Hindawi
International Journal of Intelligent Systems
Volume 2024, Article ID 3616505, 13 pages
https://doi.org/10.1155/2024/3616505

Research Article

State Feedback Control for Vehicle Electro-Hydraulic Braking Systems Based on Adaptive Genetic Algorithm Optimization

Jinhua Zhang, Lifeng Ding, and Shangbin Long

Department of Mechanical and Electrical Engineering, Guangzhou University, Guangzhou 510000, Guangdong, China

Correspondence should be addressed to Shangbin Long; sblong@gzhu.edu.cn

Received 21 March 2023; Revised 6 March 2024; Accepted 20 March 2024; Published 27 March 2024

Academic Editor: Subrata Kumar Sarker

In traditional state feedback control, the difficulty in determining the coefficient matrix is a significant factor that prevents achieving optimal control. To address this issue, this paper proposes the integration of adaptive genetic algorithms with state feedback control. The effectiveness of the proposed algorithm is validated via an electro-hydraulic braking system. Firstly, a model of the electro-hydraulic braking system is introduced. Next, a state feedback controller optimized by parameter-adaptive genetic algorithm is designed. Additionally, a penalty term is introduced into the fitness function to suppress overshoots. Finally, simulations are conducted to compare the convergence speed of parameter-adaptive genetic algorithm with genetic algorithm, ant colony optimization, and particle swarm optimization. Furthermore, the performance of the proposed algorithm, the state feedback control, and the proportional-integral control are also compared. The comparison results show that the proposed algorithm effectively accelerates the settling time of the electro-hydraulic braking system and suppresses the overshoots.

1. Introduction

The electro-hydraulic brake system (EHB) is different from the traditional automobile braking system. EHB is an advanced mechatronic system by replacing local mechanical components with electronic components [1]. EHB uses a comprehensive brake module to replace the pressure regulator and antilock braking system (ABS) and can adjust the braking pressure of four wheels independently [2, 3]. Compared with the traditional automobile braking system, EHB has the advantages of soft braking process, compact structure and fast response, which leads the development trend of automobile braking systems [4, 5].

The output pressure of an electro-hydraulic braking system (EHB) is primarily controlled by an electrical signal, typically voltage or current, regulated by an electronic control unit (ECU). When the driver presses the brake pedal, sensors on the pedal generate an electrical signal and transmit it to the EHB control unit. The control unit then calculates and adjusts the pressure of the brake fluid based on the received signal, enabling precise control of the braking force on the wheels [6, 7]. But in fact, in the process of converting electrical signals into mechanical force, due to energy transfer losses, structural defects, and external environmental interference, the actual output pressure is far from the target pressure [8, 9].

At present, there is a wide range of research focused on improving the performance of EHB. Among them, state feedback control is highly favoured by many scholars due to its applicability to multiinput multioutput systems and its simplicity. Reference [10] introduces an optimal field-oriented control using a linear quadratic regulator (LQR) for the in-wheel motor. An analytical method for determining Q and R matrices is examined. Reference [11] an analytical method is introduced to determine the coefficient matrix in the linear quadratic controller. This controller demonstrates an excellent disturbance rejection performance. In [12], a linear matrix inequality-based robust multiobjective LQR controller is designed for active trailer braking system with constraints on closed-loop pole locations and guarantee of robust stability. In [13], the lateral stability is achieved through independent motor torque control using LQR and PID. However, in the above research, the selection of coefficient matrices is based on empirical or

experimental analysis methods. These approaches heavily rely on the designer's experience and it is highly difficult to obtain the optimal value.

Recently, some nature-inspired algorithms, such as the genetic algorithm (GA) and particle swarm optimization (PSO) have been applied to obtain the global optimal parameters of LQR controllers. In [14–16], PSO, adaptive particle swarm optimization (APSO), and ant colony optimization (ACO) algorithms are used to determine the coefficient matrix in the linear quadratic controller. In [17], a comparison was made between the GA-based LQR and the traditional LQR applied to a doubly-fed asynchronous generator system. The results indicated that the GA-based LQR outperforms the traditional LQR in terms of stability and robustness. Reference [18] focuses on controlling a double inverted pendulum using pole placement and LQR control. To optimize LQR control parameters, GA and PSO are employed. Reference [19] addresses the design of LQR and PID controllers for an aircraft's pitch control system. GA is employed to optimize the parameters of both LQR and PID controllers. In the above research, most controllers use similar fitness functions, which aim to minimize the difference between the reference values and the actual values without incorporating additional constraints. In this situation, it may lead to excessive overshoots, as reported in [18, 20, 21]. In addition, the issue of GA being susceptible to get trapped in local optima has not been effectively addressed. Therefore, to prevent extreme optimization and the risk of falling into local optima during the optimization process, it is essential to incorporate penalty terms into the fitness function and thus to improve the GA performance.

Considering the above issues, a parameter-adaptive genetic algorithm-based optimization control method has been proposed. The following are the major contributions of this paper:

(1) Combining GA with SFC, this approach uses the global optimization capabilities of GA to seek the optimal coefficient matrices within state feedback control. This innovative method addresses the challenge that the appropriate coefficient matrices are difficult to be determined in traditional SFC.

(2) In order to prevent extreme optimization scenarios, this paper modifies the fitness function by incorporating penalty terms designed to suppress overshoot.

(3) The adjustment of crossover and mutation probabilities based on individual fitness is employed to achieve parameter self-adaptation, effectively accelerating the convergence speed of the GA.

The rest of this paper is organized as follows. Mathematical model of EHB is in Section 2. Then the pressure tracking controller design is presented in Section 3. In Section 4, the simulation verification and result analysis are introduced, followed by conclusions.

2. Electro-Hydraulic Braking System Model

The simplified diagram of single wheel electric-hydraulic braking is shown in Figure 1. The brake valve used in the system is proportional reducing valve. The electronic control unit of the EHB calculates the brake pressure required for the wheel based on information such as brake pedal travel, road adhesion coefficient, and vehicle speed. Then the electronic control unit controls the opening amount of the proportional reducing valve, allowing hydraulic oil to enter the brake wheel cylinder, and then brake the wheel.

The mathematical model of the EHB can be represented as follows [9]:

$$\begin{aligned} K_i K_0 u_0 - p_c A_m &= m_1 \frac{d^2 x_v}{dt^2} + B_1 \frac{dx_v}{dt} + (K_1 + K_s) x_v, \\ K_q x_v - K_c p_c &= A_p \frac{dx_p}{dt} + \frac{V_t}{4\beta_e} \frac{dp_c}{dt}, \\ p_c A_p &= m_t \frac{d^2 x_p}{dt^2} + B_p \frac{dx_p}{dt} + K_y x_p. \end{aligned} \tag{1}$$

Select status variable $x_1 = x_v$, $x_2 = x_p$, $x_3 = \dot{x_v}$, $x_4 = \dot{x_p}$, $x_5 = p_c$ and the state space expression can be written as

$$\dot{x_1} = x_3, \tag{2}$$

$$\dot{x_2} = x_4, \tag{3}$$

$$\dot{x_3} = -\frac{(K_s + K_1)}{m_1} x_1 - \frac{B_1}{m_1} x_3 - \frac{A_m}{m_1} x_5 + K_i K_0 u_0, \tag{4}$$

$$\dot{x_4} = -\frac{K_y}{m_t} x_2 - \frac{B_p}{m_t} x_4 + \frac{A_p}{m_t} x_5, \tag{5}$$

$$\dot{x_5} = \frac{4\beta_e K_q}{V_t} x_1 - \frac{4\beta_e A_p}{V_t} x_4 - \frac{4\beta_e K_c}{V_t} x_5. \tag{6}$$

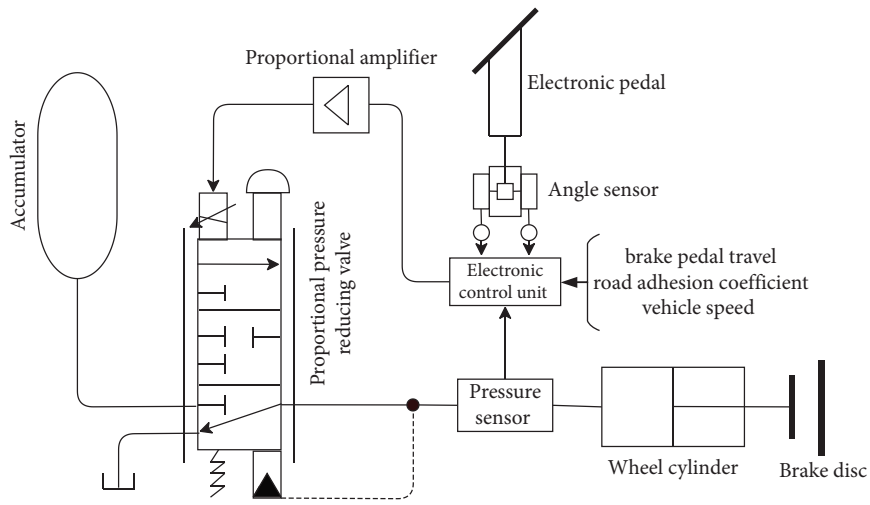

Figure 1: The principle of electro-hydraulic braking system.

The brake system model given by equations (2)–(6) can be described in the standard form of linear state equations as follows:

$$\dot{x} = \mathrm{Ax} + \mathrm{Bu}, \tag{7}$$

where

$$A = \begin{bmatrix} 0 & 0 & 1 & 0 & 0 \\ 0 & 0 & 0 & 1 & 0 \\ -\dfrac{(K_s + K_1)}{m_1} & 0 & -\dfrac{B_1}{m_1} & 0 & -\dfrac{A_m}{m_1} \\ 0 & -\dfrac{K_y}{m_t} & 0 & \dfrac{B_p}{m_t} & \dfrac{A_p}{m_t} \\ \dfrac{4\beta_e K_q}{V_t} & 0 & 0 & -\dfrac{4\beta_e A_p}{V_t} & -\dfrac{4\beta_e K_c}{V_t} \end{bmatrix}$$

$$B = \begin{bmatrix} 0 \\ 0 \\ K_i K_0 \\ 0 \\ 0 \end{bmatrix} \tag{8}$$

$$x = \begin{bmatrix} x_1 \\ x_2 \\ x_3 \\ x_4 \\ x_5 \end{bmatrix} u = u_0.$$

3. Pressure Tracking Controller Design

The performance objective of an effective braking system is to follow the desired pressure target rapidly and precisely. Therefore, the control problem for the system can be defined by the following performance function:

$$J = \frac{1}{2}\int_{t_0}^{t_f} \left[e(t)^T \mathrm{Qe}(t) + u(t)^T \mathrm{Ru}(t)\right]\mathrm{dt}, \tag{9}$$

where Q is the weight coefficient matrix with $Q = \mathrm{diag}([q_1\ q_2\ q_3\ q_4\ q_5])$; R is the control weight coefficient with $R = [r]$; $e = x_r - x$ is the error values of the state variables; t_0 and t_f are the start time and the end time, respectively. The control problem currently is: find an optimal control u to make the performance functional J take a minimum.

According to Pontryagin's minimum principle, it can be concluded that the optimal control $u(t)$ is

$$u(t) = -\mathrm{Q}^{-1}B^T P x(t) + R^{-1}B^T g, \tag{10}$$

where P and g satisfy the following equations:

$$A^T P + \mathrm{PA} - \mathrm{PBQ}^{-1}B^T P + C^T \mathrm{QC} = 0, \tag{11}$$

$$\dot{g} \approx \left[\mathrm{PBR}^{-1}B^T - A^T\right]^{-1} C^T \mathrm{Qy}_r = 0. \tag{12}$$

The values of Q and R have a significant impact on the dynamic performance of the system. When the diagonal elements of the Q takes the same value, it indicates that all state variables of the system are equally important. The larger the value, the more important the corresponding state variable. On the other hand, the R matrix is closely related to the control inputs. The larger the values of the diagonal elements, the greater the limitations imposed on the corresponding control inputs. This may lead to overshooting, but it can reduce the control effort.

After obtaining the control input $u(t)$ via solving the equations (10)–(12), it appears that a solution to the optimal control problem has been obtained. However, since the Q

and R in equation (10) are manually specified, different choices of Q and R lead to different values of $u(t)$, consequently resulting in varying cost values J. To address this issue and determine the values of Q and R that minimize J, this paper employs the GA.

GA is an optimization algorithm inspired by the natural process of evolution. It simulates the principles of biological evolution to search for optimal solutions. Figure 2 illustrates the optimization process of the GA.

This paper adopts binary encoding method. The length of binary code is related to the accuracy of solving the problem. Suppose an individual code is expressed as

$$X = a_1 a_2 a_3 a_4 \cdots a_{l-1} a_l. \tag{13}$$

The corresponding decoding method is

$$x = U_{\min} + \left(\sum_{i=1}^{l} a_i \cdot 2^{i-1} \right) \cdot \frac{U_{\max} - U_{\min}}{2^l - 1}, \tag{14}$$

where $U_{\max}$ and $U_{\min}$ represent the range of decimal values for parameters, and l is the number of bits for binary encoding.

In this paper, the individual code length is 60, and its genotype is composed of 60 binary numbers. The first fifty represent matrix Q, with a value range of 1–1000, and the last ten represent matrix R with a value range of 1–10.

In GA, The fitness function is used to assess the performance or quality of each individual solution in the problem space, quantifying the degree to which an individual is superior or inferior in solving a specific problem. Here, we first initialize the definition of the objective function as

$$F_{\text{npen}} = \int_{t_0}^{t_f} \left(\left| e_{\text{xv}} \right| + \left| e_{\text{xp}} \right| + \left| e_{\text{pc}} \right| \right) \text{dt}. \tag{15}$$

For the purpose of facilitating comparisons with other algorithms, we have modified the "roulette" selection as shown in formula (17). After the modification, individuals with smaller fitness values will have a larger selection probability.

$$P_i = \frac{\sum_{j=1}^{M} F_j}{M \cdot F_i}. \tag{16}$$

In traditional GA, the probabilities of crossover and mutation are fixed. Choosing values that are too large can result in nonconvergence, while values that are too small can lead to slow convergence. Therefore, this paper proposes a PAGA (Parameter adaptive genetic algorithm) in which the crossover and mutation probabilities for each individual are determined by the population's average fitness, individual fitness, and minimum fitness, as expressed below.

$$P_c = \begin{cases} \dfrac{k_1 (F_i - F_{\min})}{F_{\text{ave}} - F_{\min}}, & F_i \le F_{\text{ave}} \\ k_2, & F_i > F_{\text{ave}} \end{cases}, \tag{17}$$

$$P_m = \begin{cases} \dfrac{k_3 (F_i - F_{\min})}{F_{\text{ave}} - F_{\min}}, & F_i \le F_{\text{ave}} \\ k_4, & F_i > F_{\text{ave}} \end{cases}, \tag{18}$$

where P_c is the crossover probability, P_m is the mutation probability, $F_{i(i=1\ldots M)}$ is the individual fitness, $F_{\min}$ is the minimum fitness, F_{ave} is the average fitness, and $k_{i(i=1\ldots 4)}$ are adjustment parameters.

In the above, we initially define the objective function as (15), which means the sum of errors between various state variables. Because it does not impose any restrictions on the overoptimization situations, it may lead to considerable overshooting. This overshooting can have adverse effects on safety. To effectively suppress overshooting, a penalty term is introduced into the objective function.

$$F_{\text{pen}} = \int_{t_0}^{t_f} \left(\left| e_{\text{xv}} \right| + \left| e_{\text{xp}} \right| + \lambda e_{\text{pc}} \right) \text{d}t, \tag{19}$$

where $e_{\text{xv}} = x_v^{\text{ref}} - x_x$, $e_{\text{xp}} = x_p^{\text{ref}} - x_p$, $e_{\text{pc}} = p_c^{\text{ref}} - p_c$, $\lambda = \begin{cases} -a, & e_{\text{pc}} < 0 \\ 1, & e_{\text{pc}} \ge 0 \end{cases}$. a is the penalty coefficient, which will be determined in Section 4.

Figure 3 is the flow diagram of the control system proposed in this paper, which is composed of two parts. The upper part is the PAGA, and the lower part is the LQR and EHB model. At the beginning, the PAGA randomly generates an initial population consisting of 20 individuals. Each individual decodes the corresponding Q and R according to the formula (14), and then substitutes them into the simulation model of LQR and EHB one by one to get the actual response curve. Then, the fitness is calculated through the formula (19). When overshoots occur, that is, $e_{\text{pc}} < 0$, the fitness will increase significantly, thereby reducing the probability of selecting individuals with overshoots, and further suppressing the generation of overfitting. The next step will judge whether the number of evolutions reaches the set value, if not, then the next generation will be produced according to the individual fitness in the way of "roulette" selection (16), and it is possible that crossover and mutation will happen according to the set probability. Cycle the above process until the number of evolutions reaches the set end value. The individual with the highest fitness in the last generation is the optimal individual, and the decoded Q and R are the optimal weight coefficients.

To better illustrate the mechanism of how the penalty term suppresses overshoot, we provide a detailed explanation combined with the following Figure 4. We initial that the population size is 20, and the initial state of each

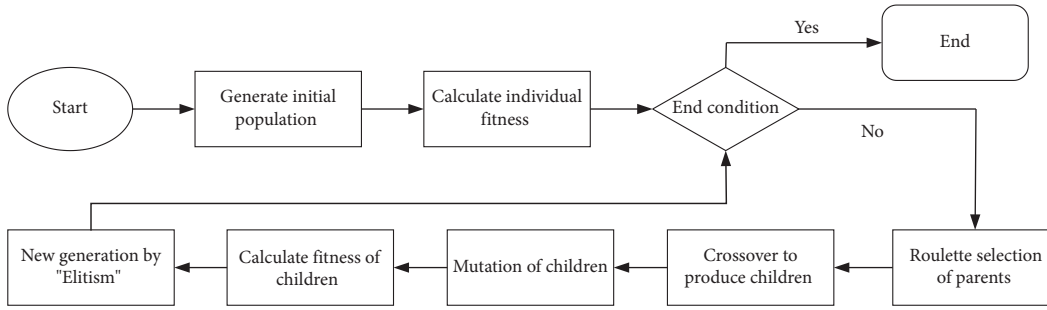

Figure 2: Genetic algorithm flowchart.

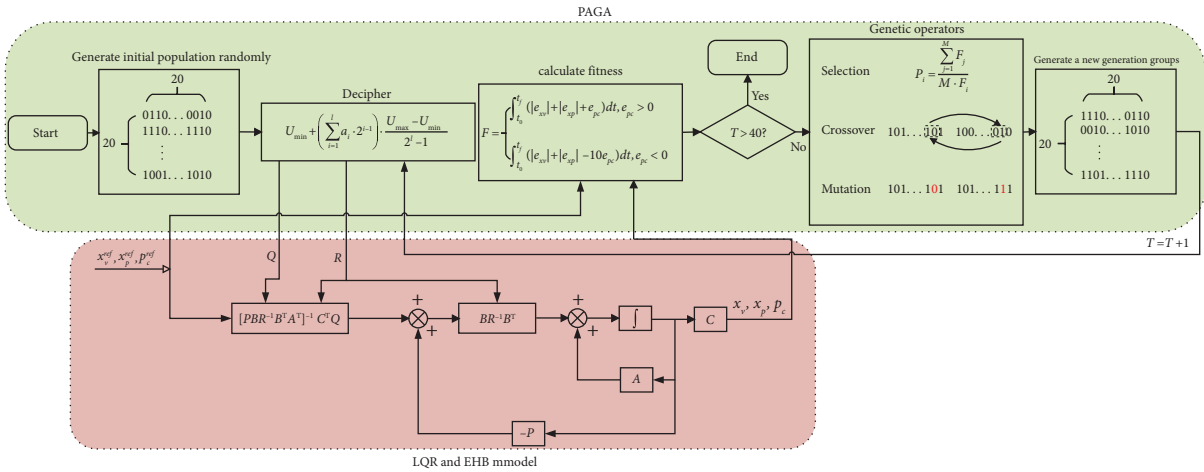

Figure 3: Control flowchart.

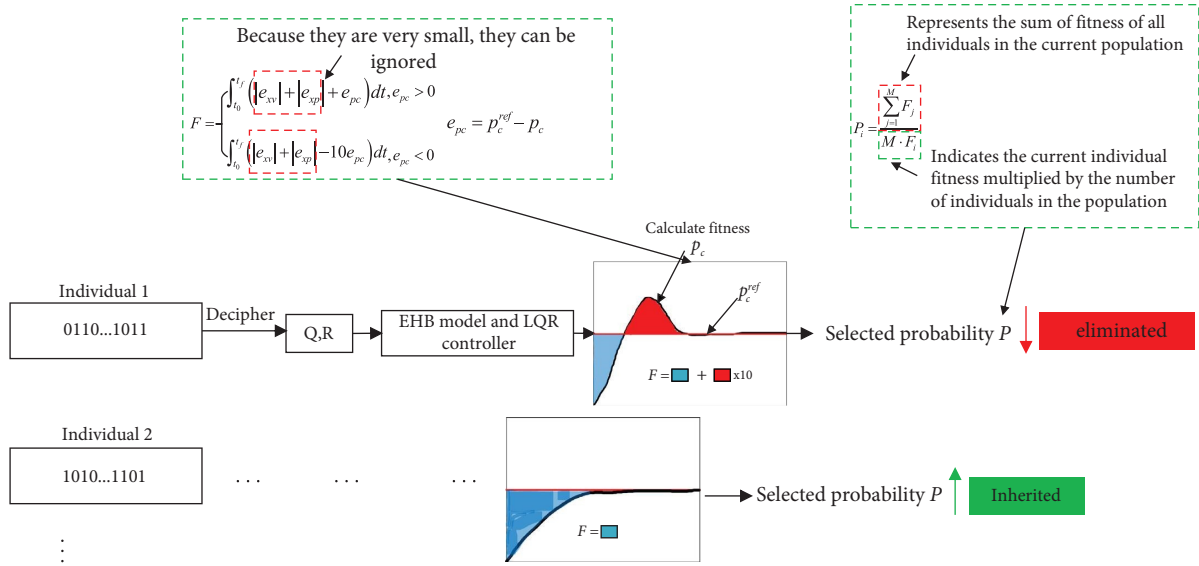

Figure 4: Schematic diagram of penalty term suppression overshoot mechanism.

individual is represented by a 60 bit binary number. After decoding, it is transformed into coefficient matrices Q (5×5) and R (1×1), which are then brought into the simulation models of LQR and EHB to obtain the response curve. The fitness of the individual is calculated using the fitness calculation formula (19). Due to the addition of the penalty term, the overshoot part will be amplified ten times, resulting in an increase in fitness and subsequently a decrease in the probability of selection and inheritance to the next generation. Over multiple generations of evolution,

individuals carrying the gene for overshoot will gradually disappear from the population, effectively preventing the occurrence of overshoot.

4. Simulation Verification

In order to verify the performance of the proposed algorithm, this paper establishes a simulation model for the EHB, and compares the performance of the GA, PAGA, PSO, and ACO algorithms. The relevant parameters of the EHB and the GA are listed in Tables 1 [2] and 2.

In this simulation, typical values were chosen for the parameters of all optimization algorithms, while the adjustment parameters $k_{i(i=1\ldots4)}$ for PAGA derived from multiple experimental trials.

To determine the appropriate penalty coefficient, we compared the effects of different penalty coefficients on suppressing overshoot by using the TO after 20 iterations as the evaluation criterion. The formula for calculating the TO is as follows:

$$\mathrm{TO} = \int_{t_s}^{t_e} \left| e_{\mathrm{pc}} \right| \mathrm{dt}, \tag{20}$$

where t_s and t_e are the time of the start overshoot and end overshoot.

Figure 5 shows the TO after 20 iterations for different values of a. It can be observed that when the value of a exceeds 10, the TO is suppressed to nearly zero. Therefore, this study selects $a = 10$. So, the $\lambda = \begin{cases} -10, & e_{\mathrm{pc}} < 0 \\ 1, & e_{\mathrm{pc}} \geq 0 \end{cases}$.

To highlight the advantages of PAGA in terms of optimization speed and the ability to overcome local optima, three additional algorithms are introduced, PSO, ACO, and GA for parameters turning process. Figure 6 is the average fitness convergence curve of four algorithms after 10 experiments with the same fitness function (15). Table 3 presents the statistical data for four algorithms across ten runs, where MF stands for "Minimum Fitness" and TItMF is the abbreviation for "Iteration Times to Minimum Fitness."

By comparing Figure 6 and Table 3, it can be observed that, under the same number of iterations, the PAGA converges much faster. PAGA finds the optimal solution at the 19th iteration, whereas PSO converges at the 36th iteration, ACO converges at the 26th iteration, and GA converges at the 20th iteration. In addition, although all three algorithms converge after 40 iterations, but they end with different minimum values. The minimum value found by PSO is 9.6762; ACO reaches a minimum value of 9.4348, while GA obtains a minimum value of 9.3583. In addition, the GA briefly encountered local optima, whereas in PAGA, this problem was effectively resolved. This suggests that during the parameter tuning process, PSO, ACO, and GA might have become trapped in local optima, while only PAGA managed to avoid local optima and find the global optimum solution. The simulation results demonstrate that the proposed parameter-adaptive GA effectively avoids local optima and accelerates convergence.

Table 1: Parameters of the electro-hydraulic braking system.

Parameters	Value
K_i	89.256
K_0	0.0746
A_m	4.52×10^{-5}
m_1	2.91×10^{-2}
B_1	3.24
K_1	824
K_s	0.0005
K_q	300
K_c	0.83×10^{-2}
A_p	80
V_t	102.5
β_e	7×10^5
m_t	30
B_p	6000
K_y	1.79×10^5

Table 2: Algorithm parameters.

Parameters	Value
PAGA	
M	20
T	40
P_c	0.5
P_m	0.005
k_1	0.8
k_2	0.5
k_3	0.1
k_4	0.75
GA	
M	20
T	40
P_c	0.5
P_m	0.005
PSO	
M	20
T	40
$c1$	1.5
$c2$	1.5
w	0.8
ACO	
M	20
T	40
ρ	0.9
p	0.2

Figure 7 shows the response curve during the autotuning procedure with PAGA. With the increase in the iteration, the response curve tends to converge more closely to the reference value. In Figure 7(a) (with no penalty term), the algorithm tends to minimize tracking errors as much as possible without imposing constraints on the overshooting behaviour. This results in extreme operating conditions in the result. However, in Figure 7(b), with the introduction of a penalty term, this risky condition is effectively suppressed.

After 40 iterations, the coefficient matrices with and without penalty term are shown below. It can be observed that the overall values of Q_{npen} are higher than Q_{pen}, while

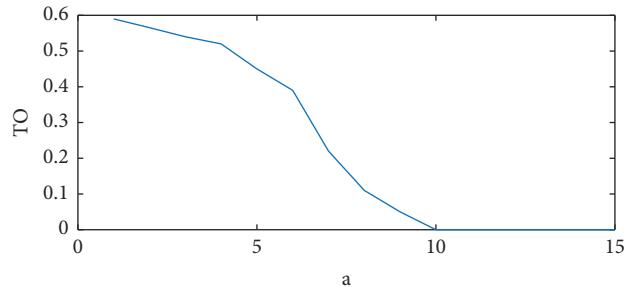

Figure 5: TO with different *a*.

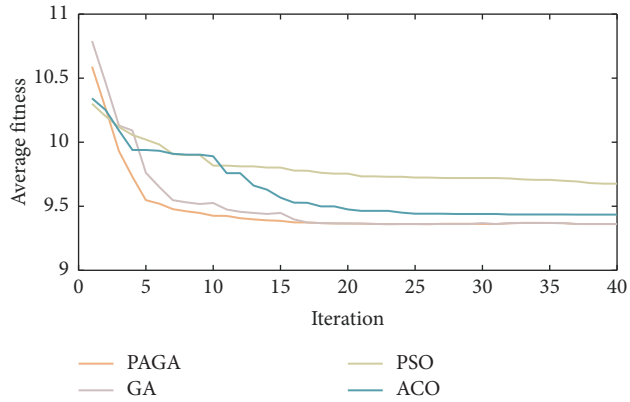

Figure 6: Iterative curves of four algorithms.

Table 3: Algorithm performance comparison table.

	PAGA		GA		PSO		ACO	
	MF	ITtMF	MF	ITtMF	MF	ITtMF	MF	ITtMF
1	9.3577	19	9.3579	19	9.4800	35	9.3689	28
2	9.3523	21	9.3575	24	9.5563	35	9.3922	17
3	9.3474	17	9.3590	17	9.5884	37	9.3789	28
4	9.3491	16	9.3582	21	9.5569	34	9.4728	20
5	9.3499	19	9.3588	20	9.7313	38	9.3812	24
6	9.3508	16	9.3575	25	9.6797	37	9.5625	34
7	9.3624	19	9.3592	21	9.7813	40	9.3758	32
8	9.3519	19	9.3582	18	9.6485	38	9.3708	21
9	9.3514	22	9.3575	17	10.0240	32	9.5051	24
10	9.3566	26	9.3589	22	9.7159	39	9.5394	37
AVG	**9.3530**	**19.4**	9.3583	20.5	9.6762	36.0	9.4348	26.5

The bold values are those yielded with the proposed method, while the unbold ones in that row are those yielded with compared methods.

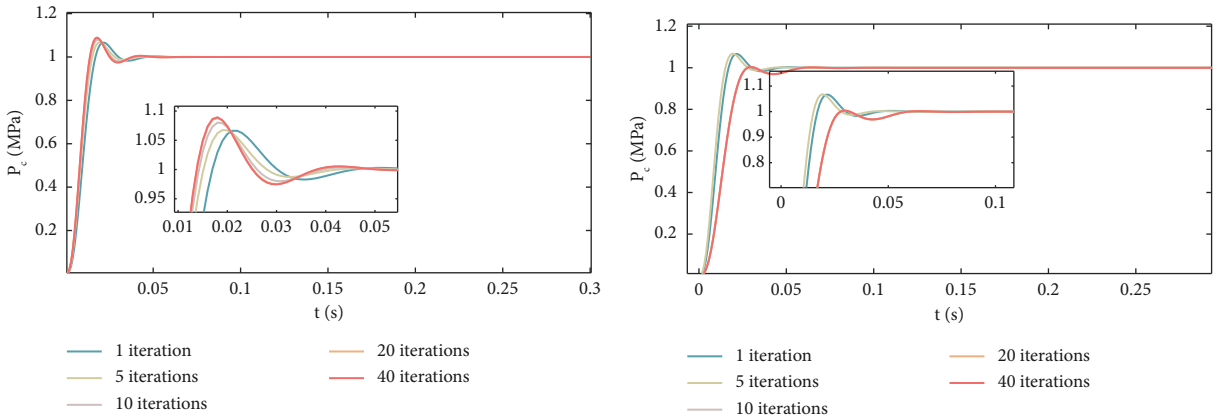

Figure 7: Response curve during auto-tuning procedure with PAGA. (a) PAGA-SFC1. (b) PAGA-SFC2.

R_{npen} is lower than R_{pen}. This indicates that a larger Q places more emphasis on state values, and a smaller R results in less emphasis on control values.

$$Q_{\text{npen}} = \begin{bmatrix} 969.7 & 0 & 0 & 0 & 0 \\ 0 & 850.9 & 0 & 0 & 0 \\ 0 & 0 & 320.2 & 0 & 0 \\ 0 & 0 & 0 & 437.5 & 0 \\ 0 & 0 & 0 & 0 & 985.2 \end{bmatrix}, R_{\text{npen}} = [1]$$

$$Q_{\text{pen}} = \begin{bmatrix} 997.1 & 0 & 0 & 0 & 0 \\ 0 & 525.4 & 0 & 0 & 0 \\ 0 & 0 & 898.5 & 0 & 0 \\ 0 & 0 & 0 & 279.3 & 0 \\ 0 & 0 & 0 & 0 & 250.1 \end{bmatrix}, R_{\text{pen}} = [5.5]. \quad (21)$$

To evaluate the stability of the proposed algorithm, we conducted tests under three different operating conditions. Additionally, a comparison was made with the traditional SFC ($Q_0 = \text{diag}([100\ 100\ 100\ 100\ 100], R_0 = \text{diag}[2]$), SFC optimized by PAGA with F_{npen} (PAGA-SFC1), SFC optimized by PAGA with F_{pen} (PAGA-SFC2), and the PID controller optimized by GA (GA-PID). Figures 7–9 depict the responses of the EHB under no load, constant load, and variable load conditions, respectively.

4.1. Constant Load Condition. When the load pressure is set to 1 MPa, all pressure tracking controllers are able to achieve zero steady-state error. As shown in Figure 8(a), the SFC shows a slower rise time compared to the other controllers and takes a longer time to reach the target value. Although GA-PI has a faster rise time than SFC, the pressure values show larger variations, and the settling time is also longer. However, PAGA-SFC1 and PAGA-SFC2 demonstrate significantly faster rise times and steady-state times. PAGA-SFC2 effectively suppresses overshoot due to the introduction of the penalty term, but it slightly increases the rise time. Figures 8(b) and 8(c) present the state values x_v and x_p for SFC, PAGA-SFC1, PAGA-SFC2, and GA-PI. In this test, both reference values are set to zero. With the help of the penalty term, PAGA-SFC1 and PAGA-SFC2 exhibit smaller oscillation amplitudes and smoother curves compared to the other two algorithms.

4.2. Sudden Load Condition. In this condition, the load pressure is initially set to 1 MPa. At 0.075 s and 0.2 s, 0.1 MPa sudden load pressure disturbances are introduced to test the disturbance rejection performance. The variations in pressure and system state responses are shown in Figure 8.

As shown in Figure 9(a), when a sudden load pressure disturbance occurs, all three SFC controllers undergo an increase or decrease in pressure, with amplitudes smaller than that of GA-PI. However, the time it takes for each of them to return to the original state is significantly different. Among them, PAGA-SFC1 and PAGA-SFC2 exhibit much faster recovery speeds. PAGA-SFC1 shows a slight overshoot after the disturbance ends, while GA-SFC2 effectively suppresses pressure overshoot due to the introduction of the penalty term. This difference can be mainly explained by the variations in the weighting matrices R associated with the control signals. The R_0 is greater than R_1 and R_2. Therefore, SFC imposes more constraints on the control signals, limiting the amount of energy given to the system. As a result, GA-SFC1 and SFC2 demonstrate better disturbance rejection characteristics compared to GA-PI, while SFC performance in this regard is less satisfactory. Figures 9(b) and 9(c) show the variations in the state variables under different algorithms. Similarly, PAGA-SFC1 and PAGA-SFC2 exhibit significantly smaller fluctuations in their ranges.

4.3. Variable Load Condition. In this simulation experiment, the load pressure is set to vary from 0.8 to 1.2 MPa according to the expression $0.2 \times \sin(50t) + 1$. The braking pressure output by the EHB is recorded in Figure 10(a). It can be observed that, compared to the two previous operating

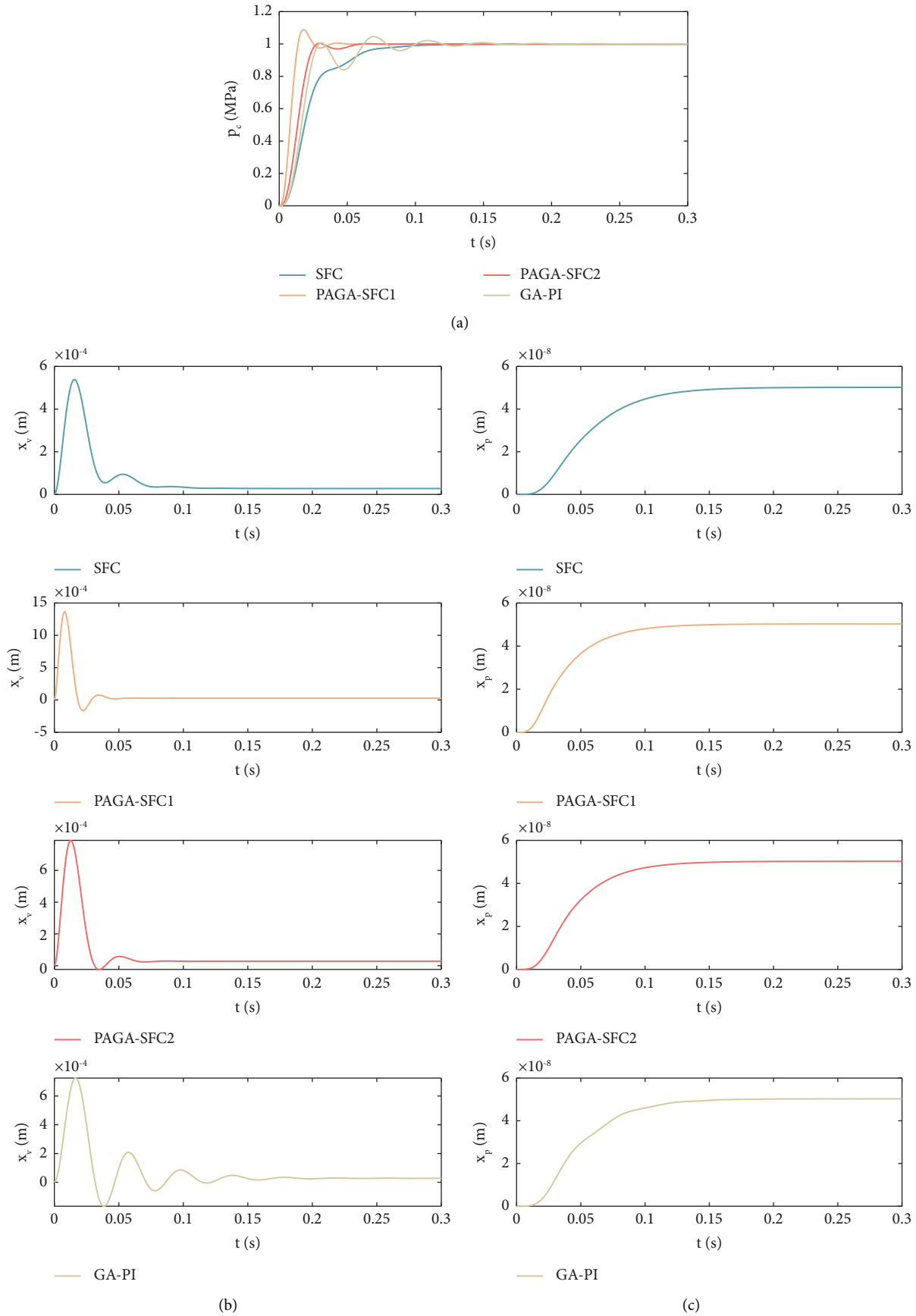

Figure 8: Responses of electro-hydraulic braking system at constant load conditions: (a) pressure, (b) armature displacement, and (c) cylinder piston displacement.

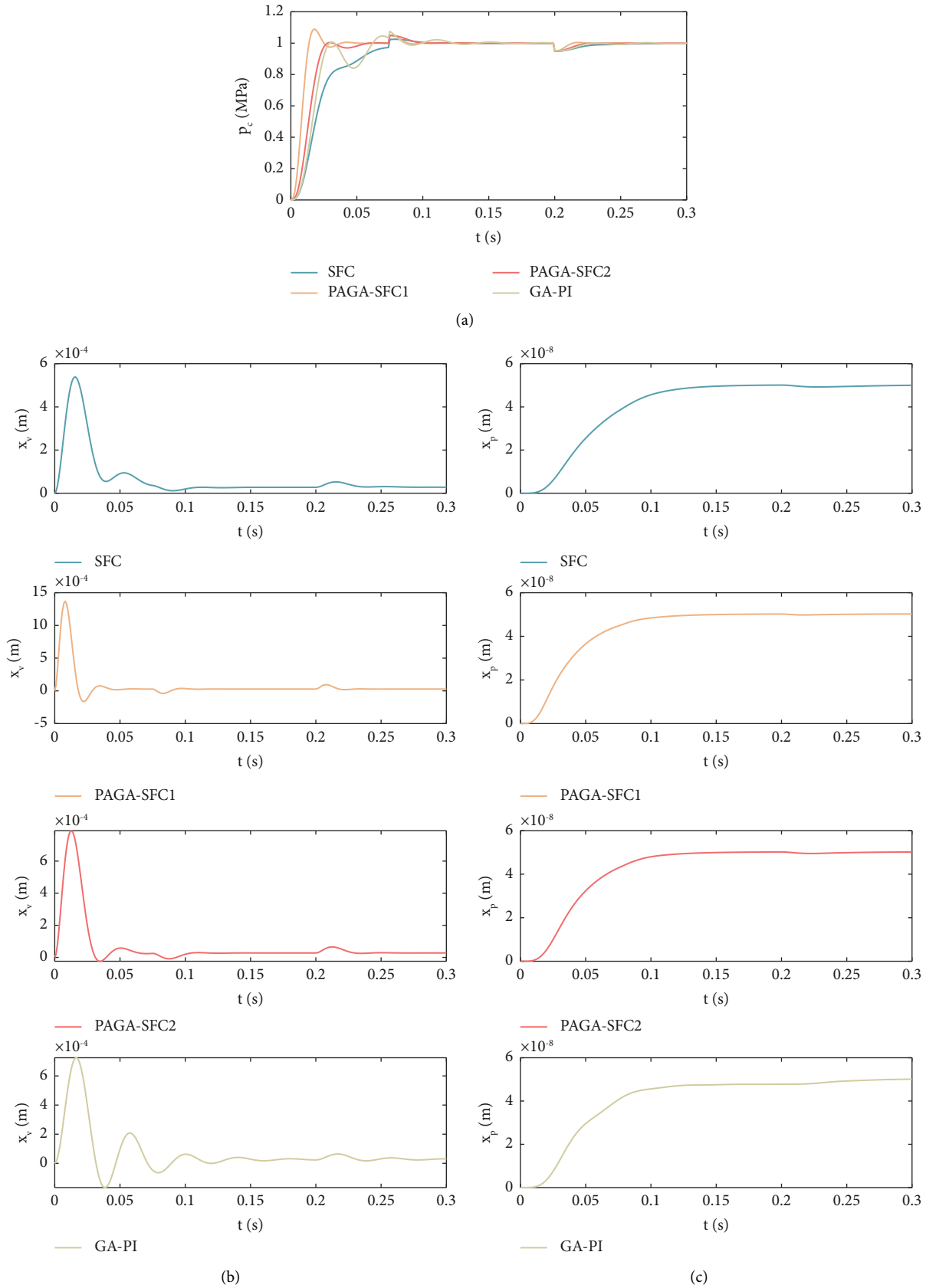

Figure 9: Responses of electro-hydraulic braking system at sudden load conditions: (a) pressure, (b) armature displacement, and (c) cylinder piston displacement.

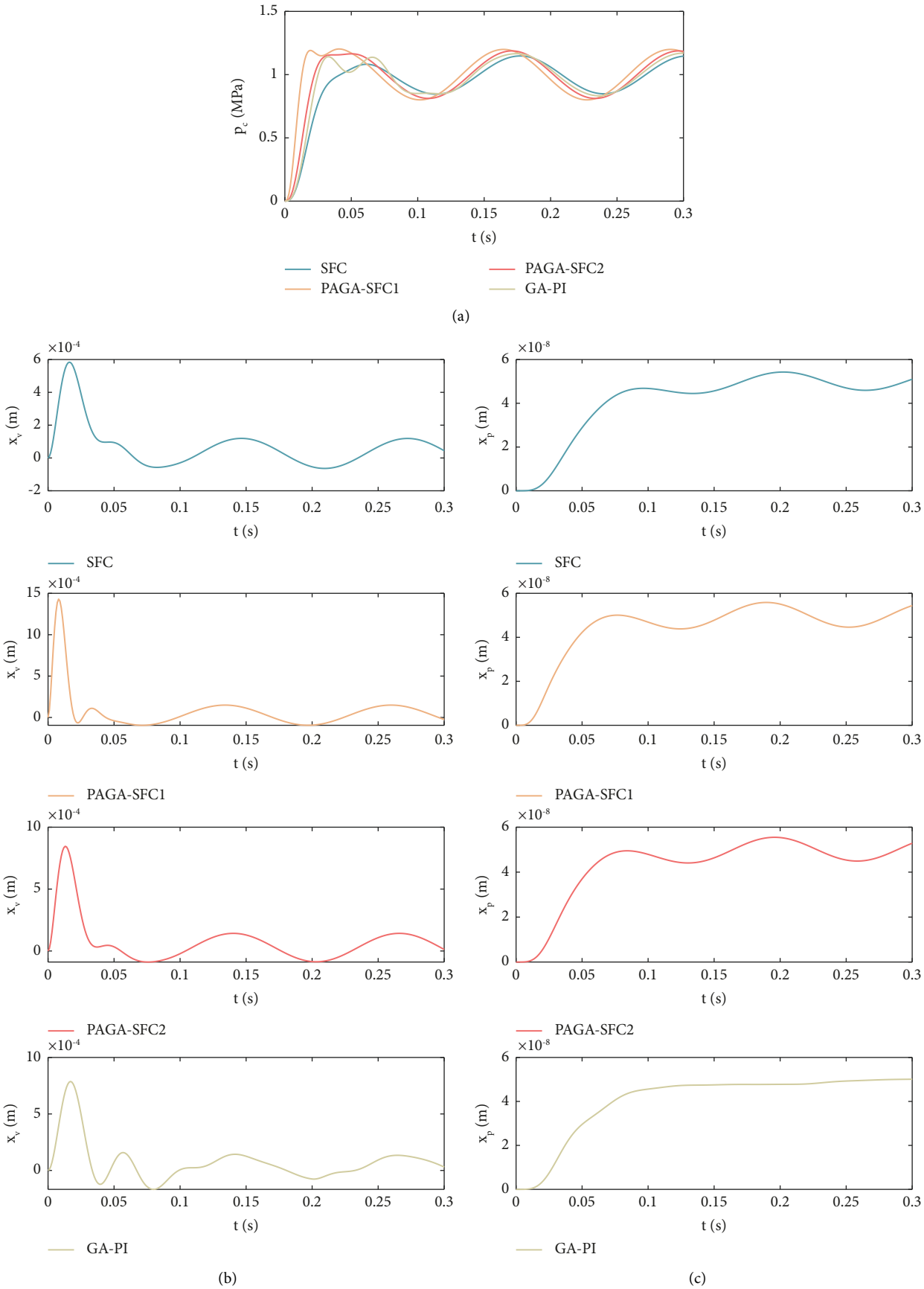

Figure 10: Responses of electro-hydraulic braking system at variable load conditions: (a) pressure, (b) armature displacement, and (c) cylinder piston displacement.

conditions, all algorithms show some steady-state error under the varying load pressure condition. However, PAGA-SFC1 and PAGA-SFC2 show significantly faster response speed and higher accuracy than the other two. This behavior can be explained by the weighting matrix Q, where larger values indicate more constraints on the corresponding variables, and q_5 is related to the pressure error. In Q_1, $q_5 = 1000$; in Q_2, $q_5 = 250.1$; while in Q_1, $q_5 = 100$. This means that PAGA-SFC1 and PAGA-SFC2 are more concerned about velocity reference tracking compared to SFC. As a result, GA-SFC1 and GA-SFC2 demonstrate better performance in following the varying load pressure.

5. Conclusions

The selection of the coefficient matrices Q and R in traditional LQR control significantly influences control performance. To address this issue, this paper proposes an approach that combines the genetic algorithm with LQR for automatic parameter tuning. In addition, to accelerate the convergence speed of the genetic algorithm, an adaptive genetic algorithm is introduced, which adjusts crossover and mutation probabilities based on individual fitness. Furthermore, to prevent overshooting, a penalty factor is incorporated into the fitness function to suppress the occurrence of overshoot. The proposed algorithm, compared to PSO and ACO, has a faster convergence speed and is less likely to fall into local optima. When compared to traditional LQR and GA-PI, it has a faster response speed and stability time.

However, there are also shortcomings in this paper. Only a single brake system model was digitally simulated without considering the impact on the control effect when the control object is the entire vehicle. Subsequent work will attempt to change the control object to the entire vehicle and verify the performance of the proposed control method under more external factors.

Abbreviations

EHB: Electro-hydraulic brake
ABS: Antilock braking system
GA: Genetic algorithm
PAGA: Parameter adaptive genetic algorithm
PSO: Particle swarm optimization
ACO: Ant colony optimization
APSO: Adaptive particle swarm optimization
SFC: State feedback control
LQR: Linear quadratic regulator
PAGA – SFC1: SFC optimized by PAGA with F_{npen}
PAGA – SFC2: SFC optimized by PAGA with F_{pen}
TO: Total overshoot

Nomenclature

MF: Minimum fitness
TItMF: Iteration times to minimum fitness
M: Size of the population
T: The number of iterations
P_m: Mutation probability
P_c: Crossover probability
$k_{i(i=1,2,3,4)}$: Adjustment parameters
$c1$: Learning factor 1
$c2$: Learning factor 2
w: Inertia weight
ρ: Pheromone evaporation factor
p: Transition probability
F_{npen}: Fitness function with no penalty
F_{pen}: Fitness function with a penalty
K_0: $K_0 = 1/R_c + r_p/\Omega^{-1}$
u_0: Amplifier output voltage (V)
p_c: Outlet pressure of pressure (MPa)
A_m: Valve spool end face area (m^2)
m_1: Equivalent mass (kg)
x_v: Armature displacement (m)
B_1: Comprehensive damping coefficient ($N \cdot S \cdot cm^{-1}$)
K_1: Spring stiffness of pressure reducing valve ($N \cdot cm^{-1}$)
K_s: Hydrodynamic stiffness coefficient ($N \cdot cm^{-1}$)
K_q: Proportional valve flow gain ($L \cdot min^{-1} \cdot cm^{-1}$)
K_c: Proportional valve flow pressure gain ($L \cdot min^{-1} \cdot Pa^{-1}$)
A_p: Piston area (cm^2)
x_p: Piston displacement (m)
V_t: The volume of hydraulic cylinder control chamber (cm^3)
β_e: Bulk elastic modulus of liquid (Pa)
m_t: The total mass of the piston and load (kg)
B_p: Viscous damping coefficient ($N \cdot m^{-1} \cdot s$)
K_y: Load spring stiffness ($N \cdot m^{-1}$).

Data Availability

The data used to support the findings of this study are available from the corresponding author upon request.

Conflicts of Interest

The authors declare that there are no conflicts of interest regarding the publication of this paper.

Acknowledgments

This research was funded by the Guangzhou Science and Technology Plan Project (202201020173 and 202201010475), the National Natural Science Foundation of China (No. 52205090), and the College-Innovation-Foundation-of Guangdong (No. 2022KQNCX058).

References

[1] L. Jiang and Q. Shi, "Electro-hydraulic braking dynamics for pressure demand control of brake-by-wire system," *Proceedings of the Institution of Mechanical Engineers- Part D: Journal of Automobile Engineering*, vol. 238, no. 4, pp. 735–748, 2022.

[2] L. I. Zhu-fang, "Pressure control of Electro- hydraulic brake for construction vehicle based on LQR," *Chinese Hydraulics and Pneumatics*, vol. 01, p. 109, 2015.

[3] J. Hong, H. Zhang, and X. Xu, "Thermal fault prognosis of lithium-ion batteries in real-world electric vehicles using self-attention mechanism networks," *Applied Thermal Engineering*, vol. 226, Article ID 120304, 2023.

[4] Z. Zhang, T. Zhang, J. Hong, H. Zhang, and J. Yang, "Energy management strategy of a novel parallel electric-hydraulic hybrid electric vehicle based on deep reinforcement learning and entropy evaluation," *Journal of Cleaner Production*, vol. 403, Article ID 136800, 2023.

[5] J. Hong, T. Zhang, Z. Zhang, and H. Zhang, "Investigation of energy management strategy for a novel electric-hydraulic hybrid vehicle: self-adaptive electric-hydraulic ratio," *Energy*, vol. 278, Article ID 127582, 2023.

[6] J. Zhang, W. Sun, and Z. Feng, "Vehicle yaw stability control via H∞ gain scheduling," *Mechanical Systems and Signal Processing*, vol. 106, pp. 62–75, 2018.

[7] J. Zhang, W. Sun, and H. Du, "Integrated motion control scheme for four-wheel-independent vehicles considering critical conditions," *IEEE Transactions on Vehicular Technology*, vol. 68, no. 8, pp. 7488–7497, 2019.

[8] J. Zhang, W. Sun, Z. Liu, and M. Zeng, "Comfort braking control for brake-by-wire vehicles," *Mechanical Systems and Signal Processing*, vol. 133, Article ID 106255, 2019.

[9] M. Lin, G. Yao, and W. Qu, "Simulation and experiment of electro-hydraulic braking system of construction vehicles," *Transactions of the Chinese Society of Agricultural Engineering*, vol. 27, p. 11, 2011.

[10] C. J. Meirinho, A. Bartsch, J. de Oliveira, and M. S. M. Cavalca, "An optimal MIMO control approach for PMSM drives," in *Proceedings of the Brazilian Power Electron. Conf. (COBEP)*, pp. 1–6, Juiz de Fora, Brazil, November 2017.

[11] M. Brasel, "A gain-scheduled multivariable LQR controller for permanent magnet synchronous motor," in *Proceedings of the 19th Int. Conf. Methods Models Auto. Robot. (MMAR)*, pp. 722–725, Midzyzdroje, Poland, September 2014.

[12] M. Sever, "Active trailer braking system design with linear matrix inequalities based multi-objective robust LQR controller for vehicle-trailer systems," in *Proceedings of the 2016 IEEE Intelligent Vehicles Symposium (IV)*, IEEE, Gotenburg, Sweden, June 2016.

[13] I. Yogurtcu, S. Solmaz, and S. Çaglar Baslamish, "Lateral stability control based on active motor torque control for electric and hybrid vehicles," in *Proceedings of the 2015 IEEE European Modelling Symposium (EMS)*, IEEE, Madrid, Spain, October 2015.

[14] J. Fang, "The LQR controller design of two-wheeled self-balancing robot based on the particle swarm optimization algorithm," *Mathematical Problems in Engineering*, vol. 2014, Article ID 729095, 6 pages, 2014.

[15] E. Vinodh Kumar, G. S. Raaja, and J. Jerome, "Adaptive PSO for optimal LQR tracking control of 2 DoF laboratory helicopter," *Applied Soft Computing*, vol. 41, pp. 77–90, 2016.

[16] B. Ata and R. Coban, "Artificial bee colony algorithm based linear quadratic optimal controller design for a nonlinear inverted pendulum," *International Journal of Intelligent Systems and Applications in Engineering*, vol. 3, no. 1, pp. 1–6, 2015.

[17] R. Bhushan, K. Chatterjee, and R. Shankar, "Comparison between GAbased LQR and conventional LQR control method of DFIG wind energy system," in *Proceediings of the 3rd Int Conf On Recent Advances in Info Technology (RAIT)*, pp. 214–219, Dhanbad, India, March 2016.

[18] M. K. Habib and S. A. Ayankoso, "Modeling and control of a double inverted pendulum using LQR with parameter optimization through GA and PSO," in *Proceediings of the 2020 21st International Conference on Research and Education in Mechatronics (REM)*, IEEE, Cracow, Poland, December 2020.

[19] J. Ohri, "GA tuned LQR and PID controller for aircraft pitch control," in *Proceediings of the 2014 IEEE 6th India International Conference on Power Electronics (IICPE)*, IEEE, Kurukshetra, India, December 2014.

[20] T. Tarczewski and L. M. Grzesiak, "An application of novel nature inspired optimization algorithms to auto-tuning state feedback speed controller for PMSM," *IEEE Transactions on Industry Applications*, vol. 54, no. 3, pp. 2913–2925, 2018.

[21] T. Tarczewski and L. M. Grzesiak, "Constrained state feedback speed control of PMSM based on model predictive approach," *IEEE Transactions on Industrial Electronics*, vol. 63, no. 6, pp. 3867–3875, 2016.